

RECENT RESULTS FOR THE FERRITICS ISOTOPIC TAILORING (FIST) EXPERIMENT - D. S. Gelles, M. L. Hamilton, B. M. Oliver and L. R. Greenwood (Pacific Northwest National Laboratory),* S. Ohnuki (University of Hokkaido, Japan), K. Shiba (JAERI Tokai, Japan), Y. Kohno (Muroran Institute of Technology, Japan), A. Kohyama (Kyoto University, Japan) and J. P. Robertson (Oak Ridge National Laboratory)

OBJECTIVE

The objective of this effort is to quantify transmutation-induced irradiation hardening response in isotopically tailored ferritic alloys following irradiation at 300, 400 and 500°C in order to better understand behavior in this alloy class.

SUMMARY

The results of shear punch testing, microstructural examination, and hydrogen and helium analyses performed on irradiated isotopically tailored alloys are reported for specimens irradiated in the HFIR JP20 experiment.

PROGRESS AND STATUS

Introduction

Post-irradiation deformation response, microstructural change, and transmutation induced gas generation of hydrogen and helium has been reported based on measurements of two specimen conditions of an isotopically tailored alloy containing ^{54}Fe addition to the F82H composition in order to study hydrogen and helium embrittlement in single variable experiments.^{1,2} Those results were shown to indicate that transmutation-induced hydrogen may play an important role in irradiation embrittlement.³ Recently, three more isotopically tailored specimen conditions irradiated in the HFIR JP20 experiment in positions 6, 9 and 7 corresponding to ~8 dpa at 300, 400 and 500°C were made available for examination. This report is intended to provide post-irradiation deformation response base on the shear punch technique, microstructural examination and transmutation induced gas content for these three conditions.

Experimental Procedures

Two transmission electron microscopy (TEM) disks of ^{54}Fe isotopically tailored F82H were obtained from each of the HFIR JP20 experiment positions 6, 9 and 7. The experimental design of the JP20 experiment is described in reference 4, specimen loading is documented in reference 5 and irradiation history and neutron dosimetry can be found in reference 6. The corresponding specimen identification codes are: C601 and C602 for position 6 at 300°C, C605 and C606 for position 9 at 400°C, and C609 and C610 for position 7 at 500°C. One disk for each condition was tested by shear punching and then prepared as a thin foil using the central 1 mm disk created during shear punch testing as described previously.^{1,2} The outer ring that remained was then sectioned and used for hydrogen and helium analyses using procedures described previously.⁷

* Pacific Northwest National Laboratory (PNNL) is operated for the U.S. Department of Energy by Battelle Memorial Institute under contract DE-AC06-76RLO-1830.

Results

Results of shear punch testing are provided in Table 1 and the test curves are shown in Figure 1. Table 1 and Figure 1 include results from previous tests. From these results, it can be shown that irradiation at 500°C produces only slightly higher hardening than in the unirradiated condition whereas irradiation at 300 and 400°C produces similar levels of hardening, intermediate between that due to irradiation at 250°C to 2.4 dpa and irradiation at 300°C to 34 dpa.

Table 1. Results of shear punch testing at room temperature.

ID	MATERIAL	CONDITION	τ_{ys}	τ_{ms}
A943-5	F82H IEA	Unirradiated	340,345,350	458,469,473
F191-3	F82H STD	Unirradiated	325,350,360	476,482,492
C103	F82H STD	300°C, 34 dpa	580	609
FN91-3	F82H ^{54}Fe	Unirradiated	390,400,406	519,520,522
FN51-2	F82H ^{54}Fe	250°C, 2.3 dpa	500,520	602,608
C601	F82H ^{54}Fe	300°C, 7.3 dpa	575	655
C605	F82H ^{54}Fe	400°C, 7.3 dpa	595	660
C609	F82H ^{54}Fe	500°C, 7.5 dpa	400	540
C603	F82H ^{54}Fe	300°C, 34 dpa	600	738
C203	F82H B-F82H	300°C, 34 dpa	470	656

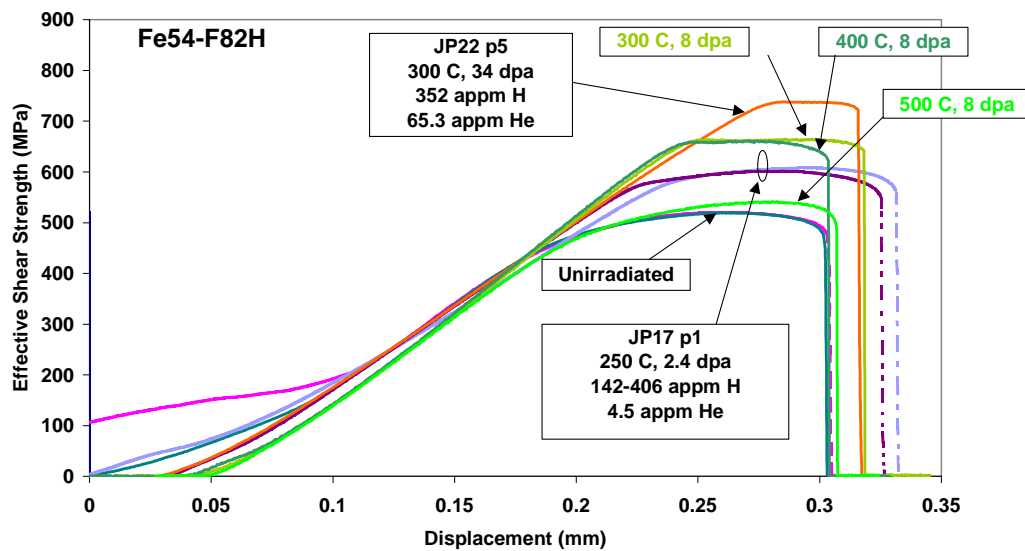


Figure 1. Shear punch test traces for FIST specimens containing ^{54}Fe .

Helium concentrations have been measured for specimens C601, C605 and C609 and the results are provided in Table 2 along with results from previous FIST measurements. Hydrogen concentrations were also measured and the results are provided in Table 3 along with previous results. Helium levels for the three conditions are found to be similar indicating that changes in irradiation temperature did not affect helium retention. Hydrogen levels varied with temperature, the highest levels found after irradiation at 400°C, with lower hydrogen following irradiation at 300°C and the lowest following irradiation at 500°C.

Table 2. Helium concentrations in FIST samples.

Sample	Material	Irradiation Conditions	Mass ^a (mg)	Measured ⁴ He (10 ¹⁴ atoms)	Helium Concentration (appm) ^b	
					Measured	Average ^c
FN51-2	F82H+ ⁵⁴ Fe	JP17/250°C	1.073	0.5278	4.550	4.52
			1.603	0.7765	4.481	±0.05
C103	F82H+ ⁰ Fe	JP22/300°C	1.567	3.684	21.89	21.8
			1.892	4.407	21.69	±0.1
C203	F82H+ ¹⁰ B	JP22/300°C	0.851	29.81	325.9	320
			1.864	63.05	314.7	±8
C603	F82H+ ⁵⁴ Fe	JP22/300°C	1.047	7.348	64.92	64.8
			1.711	11.96	64.66	±0.2
C601	F82H+ ⁵⁴ Fe	JP22/300°C	1.042	1.179	10.47	10.4
			1.342	1.507	10.39	±0.1
C605	F82H+ ⁵⁴ Fe	JP22/400°C	0.626	0.6937	10.25	10.2
			1.246	1.372	10.19	±0.1
C609	F82H+ ⁵⁴ Fe	JP22/500°C	0.459	0.5625	11.34	11.2
			1.090	1.308	11.10	±0.2

^aMass of specimen for analysis. Mass uncertainty is ±0.002 mg.

^bHelium concentration in atomic parts per million (10⁻⁶ atom fraction) with respect to the total number of atoms in the specimen.

^cMean and standard deviation (1σ) of duplicate analyses.

Microstructural examinations have been performed on each of the conditions available. Examples of these microstructures at low magnification are provided in Figure 2, with one example following irradiation at 300°C, two examples following irradiation at 400°C and one example following irradiation at 500°C. All show typical martensite lath structure decorated with M₂₃C₆ carbide. Of particular note are the voids showing at low density following irradiation at 400°C (and therefore two examples are given). Also, it is possible but difficult to quantify, that following irradiation at 500°C precipitate decoration of lath boundaries is more complete.

Table 3. Hydrogen concentrations in FIST samples.

ID	Material	Irradiation Conditions	Mass ^a (mg)	Measured Hydrogen (10 ¹⁵ at)	Hydrogen Concentration (appm) ^c		Avg ^d
					Measured	Corrected ^b	
FN92	F82H+ ⁵⁴ Fe	Unirradiated	2.112	1.16	51	-	44
			2.916	1.34	43	-	±6
			2.699	1.29	44	-	
			1.081	0.875	37	-	
FN51-1	F82H+ ⁵⁴ Fe	JP17/250°C	2.523	15.1	554	510	406
			3.228	8.92	256	212	±151
			0.840	5.29	583	539	
			1.551	6.78	405	361	
FN51-2	F82H+ ⁵⁴ Fe	JP17/250°C	2.834	3.82	125	81	142
			3.276	8.70	246	202	±86
C603	F82H+ ⁵⁴ Fe	JP22/300°C	0.723	3.10	398	354	352
			0.924	4.24	425	381	±21
			1.038	4.33	386	342	
			1.221	4.96	376	332	
C601	F82H+ ⁵⁴ Fe	JP22/300°C	1.734	17.9	954	910	845
			2.082	18.5	824	780	±92
C605	F82H+ ⁵⁴ Fe	JP22/400°C	1.819	26.7	1360	1316	1280
			2.208	30.7	1287	1243	±52
C609	F82H+ ⁵⁴ Fe	JP22/500°C	1.915	15.4	746	702	630
			2.549	16.6	601	557	±103

^aMass of specimen for analysis. Mass uncertainty is ±0.002 mg.

^bCorrected for hydrogen measured in unirradiated control material, FN92.

^cHydrogen concentration in atomic parts per million (10⁻⁶ atom fraction) with respect to the total number of atoms in the specimen.

^dMean and standard deviation (1σ) of replicate (corrected) analyses.

The dislocation and bubble structures were studied in greater detail by examining these microstructures in dark field under dislocation contrast. Examples are provided in Figure 3 comparing a region of interest for each condition under $g=011$ and 200 dark field along with a bright field image, for C601 and C605 in void contrast and for C609 in dislocation contrast. Figure 3 shows that the dislocation structure changes with irradiation temperature, loop size increasing and density decreasing with increasing temperature. However, other differences can be identified. For example, $a\langle 100 \rangle$ Burgers vectors predominate following irradiation at 400°C, but are not present following irradiation at 500°C and may not be present following irradiation at 300°C. This is demonstrated most straightforwardly in Figure 3e) where horizontal features (perpendicular to the operating 200 diffraction vector) are of Burgers vector $a[100]$ whereas all other dislocation line segments (in weaker contrast) are of type $\frac{a}{2}\langle 111 \rangle$. Also of note are smaller equiaxed features in Figures 3a and b) about 5 nm in diameter. These may be small loops or gas bubbles, but because they are not visible in Figure 3c), it is expected that they are due to precipitation, possible α' or carbide. Finally, bubbles on the order of 5 nm in diameter may be seen in Figure 3c) but the density is apparently low.

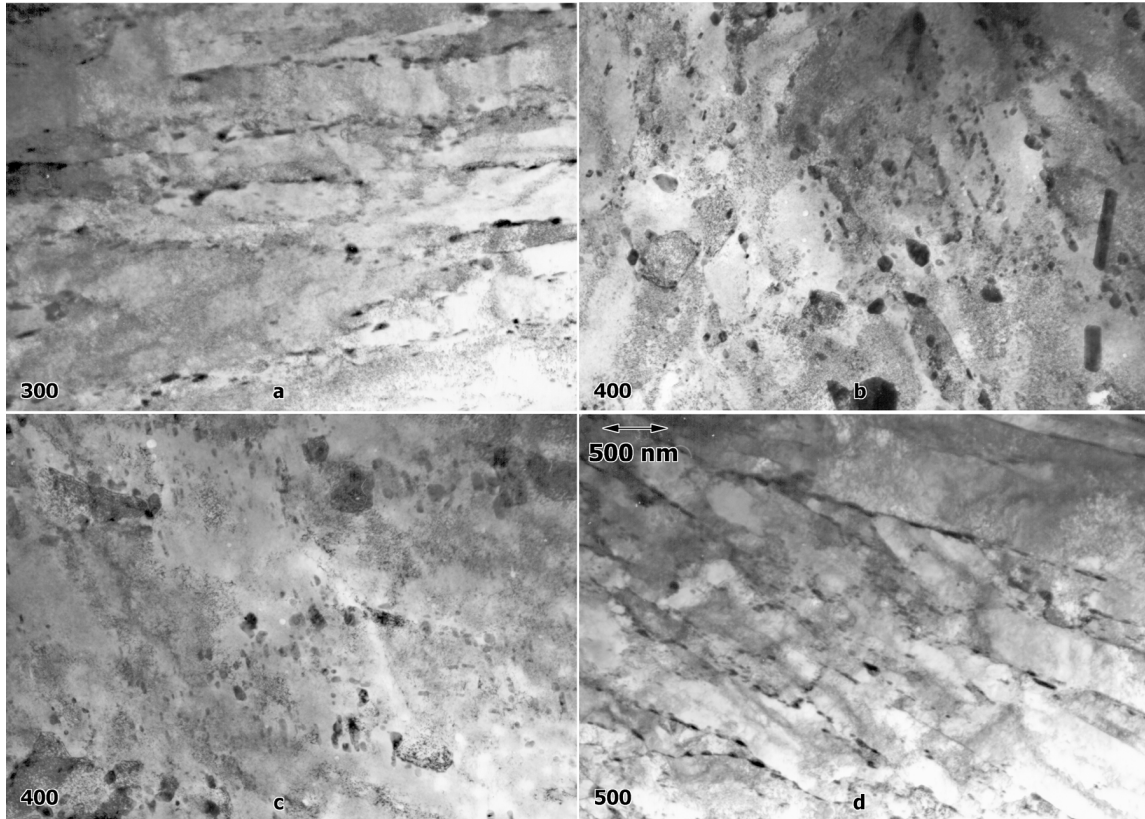


Figure 2. Low magnification examples of microstructures in C601 a), C605 b) and c), and C609 d) .

Discussion

Irradiation hardening response is plotted as a function of dose and temperature for effective shear yield and maximum strength, respectively, in Figures 4 through 7. Data from samples C601, C605 and C609 is labeled 300 C, 400 C and 500 C, respectively. Behavior of strength as a function of dose in Figures 4 and 6 follows expected behavior for 300 and 400°C but strength following irradiation at 500°C is much lower. This is further demonstrated in Figures 5 and 7. Therefore, it is reasonable to directly compare response following irradiation at 250, 300 and 400°C. Note that this response is typical of irradiation hardening without the influence of transmutation-induced gases.

In order to identify effects of He and H produced by transmutation during irradiation, it is best to plot hardening behavior as a function of He and H as shown previously.⁸ Therefore, the change in effective shear strength is shown plotted as a function of He and H content in Figure 8. Figure 8 includes previous results as well as results for conditions C601, C605 and C609. From Figure 8, several conclusions can be drawn. Strength changes found previously as a function of He are similar to that in Figure 8, except for results at 500°C. Therefore, conclusions drawn previously may still apply: that it is possible that there is no effect of He on yield response whereas a bi-linear response can be identified for the maximum strength if one excludes results at 500°C. Bi-linear response is indicated because zero hardening is imposed for zero He. Results as a function of H must be interpreted differently. Data for C601, C605 and C609 give very different irradiation hardening behavior as a function of H compared to response found previously, with no straightforward correlation evident.

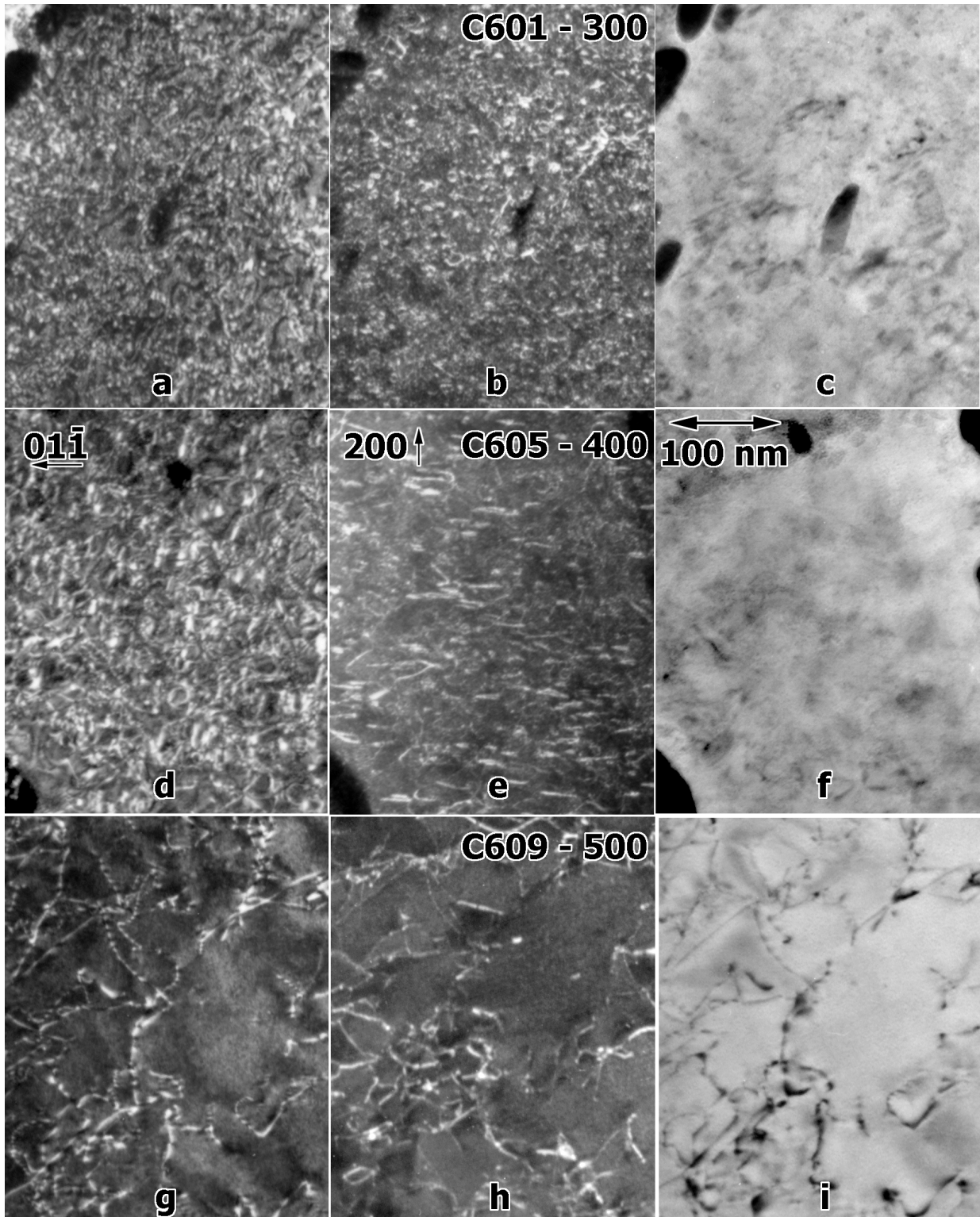


Figure 3. Dislocation structure in conditions C601, C605 and C609 shown in $\bar{g} = 011$, 200 and bright field contrast, respectively.

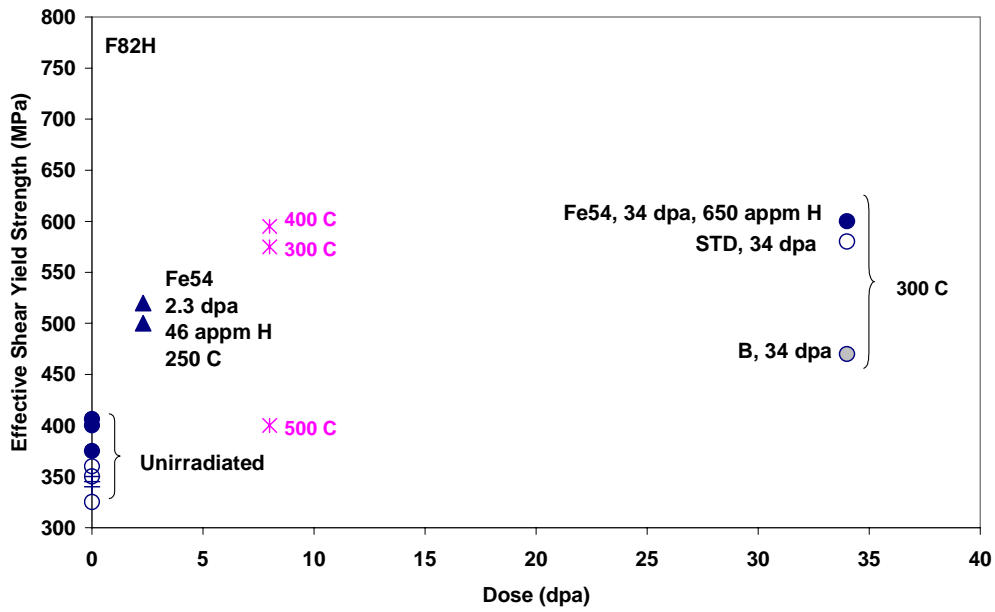


Figure 4. Effective Shear Yield Strength as a function of dose for isotopically tailored F82H.

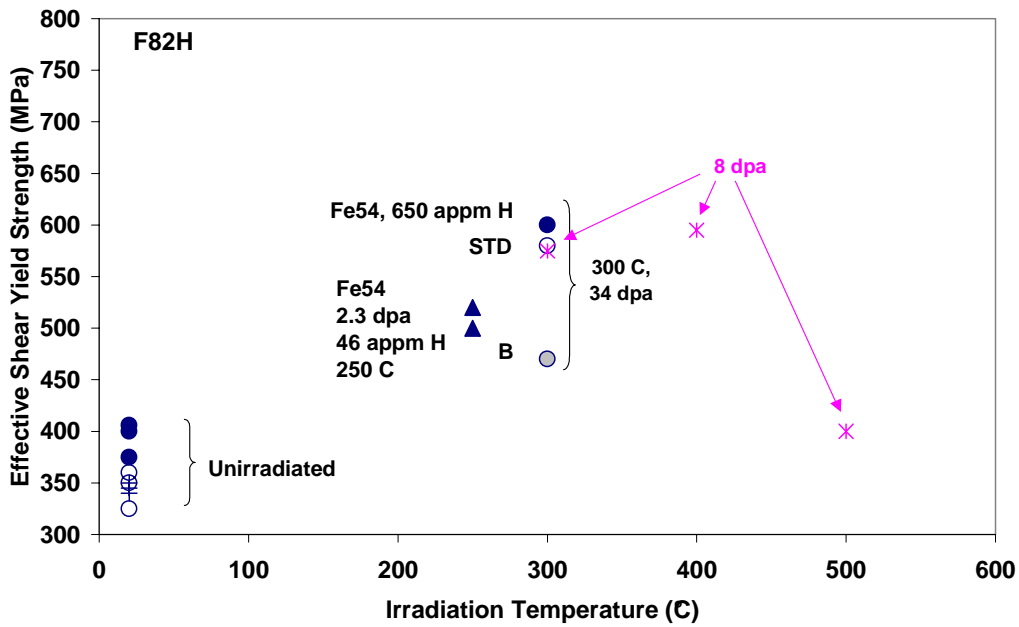


Figure 5. Effective Shear Yield Strength as a function of temperature for isotopically tailored F82H.

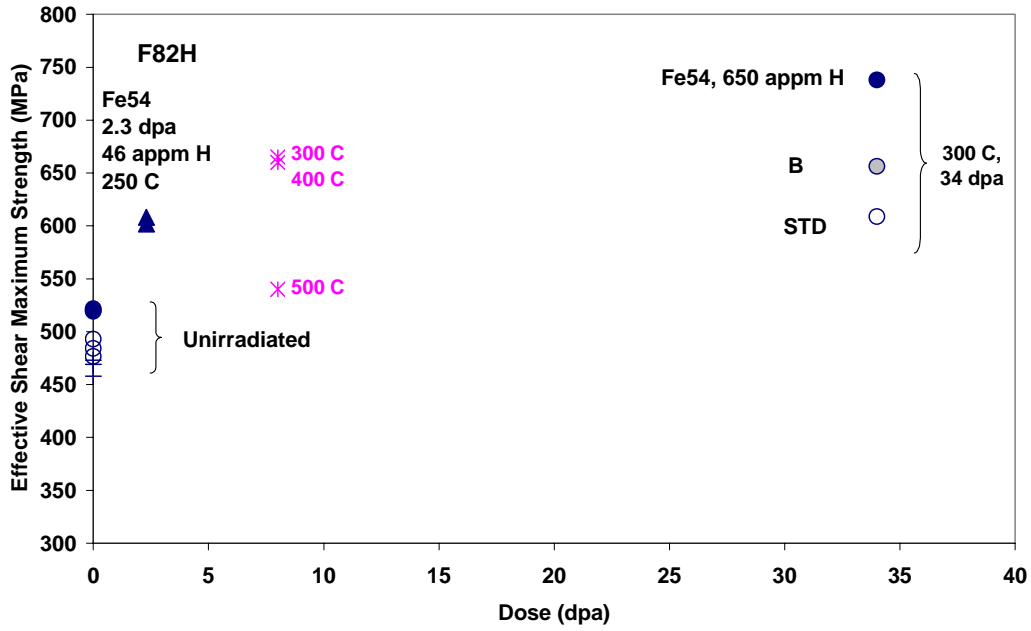


Figure 6. Effective Shear Maximum Strength as a function of dose for isotopically tailored F82H.

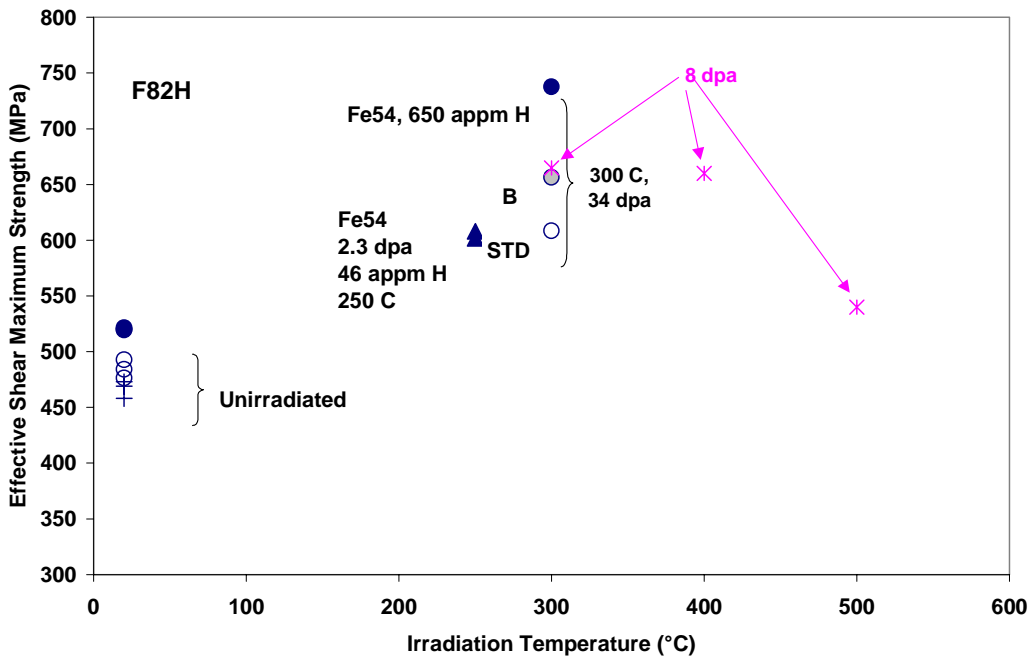


Figure 7. Effective Shear Maximum Strength as a function of temperature for isotopically tailored F82H.

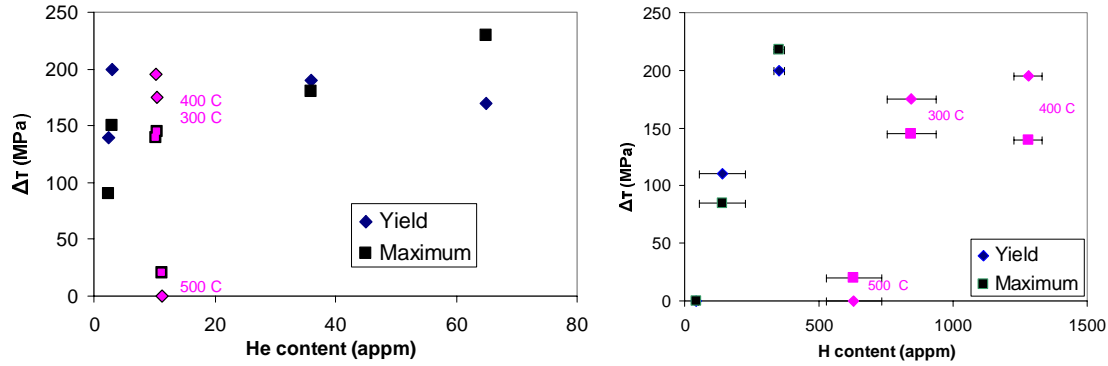


Figure 8. Change in τ_{ys} and τ_{ms} due to irradiation as a function of a) He content and b) H content for FIST alloys.

It must be noted that the measurements of helium in specimens C601, C605 and C609 fit predicted behavior whereas measurements for H are considerably higher than expected. This is demonstrated in Figure 9 a) and b) showing He and H measured levels in comparison with prediction. The He measurements agree with calculations that take into account increased helium production from both ^{54}Fe and transmutation to ^{55}Fe (Reference 7), as shown in Figure 9a. Calculations for H, which also take into account the Fe isotopic cross sections and transmutation are compared with the data in Figure 9b. Most of the H measurements are higher than predicted, although an earlier measurement at a higher dose is considerably below the calculated value. The earlier data was interpreted to indicate that H can be lost during irradiation whereas the present data indicated that not only is H not lost, it can be generated at higher than expected rates.

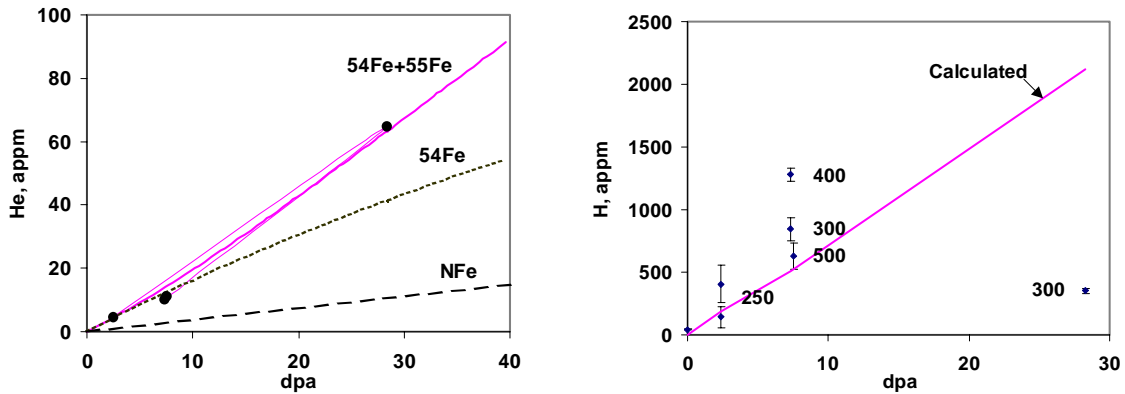


Figure 9. Helium and hydrogen production in ^{54}Fe isotopically tailored F82H, measurement verses prediction.

Only one of the two specimens available for examination has been used. Therefore, consideration is being given to using the remaining specimens for remeasurement of H. Also, this work would be enhanced greatly if control conditions (those without ^{54}Fe) were available. Then it should be possible to objectively account for effects of transmutation-induced He and H. Unfortunately, it has not yet been possible to obtain such control conditions.

Conclusions

Three conditions of isotopically tailored F82H irradiated in the HFIR JP20 experiment have been tested, examined by TEM, and analyzed for He and H content in order to quantify irradiation hardening due to transmutation-induced helium and hydrogen.

Hardening due to irradiation is found following irradiation at 300 and 400°C, that is intermediate between that at lower and higher dose, but hardening is negligible following irradiation at 500°C.

Microstructural examinations show typical behavior of irradiation as a function of irradiation temperature, with moderate swelling after 400°C irradiation but few bubbles after irradiation at 300°C.

Correlations of change in hardening with He and H content show little indication of transmutation-induced hardening, but measured H levels do not agree with predictions and therefore H production and analysis requires further study.

FUTURE WORK

Uses for the duplicate unused specimens from this study will be considered. Availability of other specimens pertinent to this work will be sought. A more complete test is being considered for future HFIR irradiation.

REFERENCES

- [1] M. L. Hamilton, D. S. Gelles, S. Ohnuki, K. Shiba, Y. Kohno, and A. Kohyama, DOE/ER-0313/25 (1999) 136.
- [2] D. S. Gelles, S. Ohnuki, K. Shiba, Y. Kohno, A. Kohyama, J. P. Robertson, and M. L. Hamilton, DOE/ER-0313/25 (1999) 143.
- [3] S. Ohnuki, Y. Kohno, A. Kohyama, K. Shiba, D. S. Gelles, M. L. Hamilton, and J. P. Robertson, presented at ICFRM-9 in Colorado Springs October 1999, paper 7.04.
- [4] J. E. Pawel, and R. L. Senn, DOE/ER-0313/12 (1992) 15.
- [5] J. E. Pawel, A. W. Longest, R. L. Senn, K. Shiba, D. W. Weatherly, and R. G. Sitterson, DOE/ER-0313/15 (1994) 3.
- [6] L. R. Greenwood and C. A. Baldwin, DOE/ER-0313/18 (1998) 305.
- [7] L. R. Greenwood, B. M. Oliver, S. Ohnuki, K. Shiba, Y. Kohno, A. Kohyama, J. P. Robertson, J. W. Meadows and D. S. Gelles, J. Nucl. Mater. 283-287 (2000) 1438.
- [8] D. S. Gelles, M. L. Hamilton, B. M. Oliver, and L. R. Greenwood, DOE/ER-0313/27 (2000) 149.